Accurate depth-independent determination of acoustic backscatter coefficients with focused transducers

Timothy J. Hall,[a] Ernest L. Madsen, James A. Zagzebski, and Evan J. Boote[b]
Department of Medical Physics, University of Wisconsin, Madison, Wisconsin 53706

(Received 12 December 1987; accepted for publication 22 February 1989)

The accuracy of a method of data reduction for determining acoustic backscatter coefficients was tested using focused transducers and narrow-band pulses. Two phantoms with well-defined scattering properties were the bases of the tests, one having low attenuation and one with tissue-mimicking attenuation. The experimentally determined backscatter coefficients were found to be independent of transducer-to-scattering-volume distance and to agree very well with theoretical values, typically within 10%.

PACS numbers: 43.35.Yb, 43.35.Bf

INTRODUCTION

The derivation of a method of data reduction for accurately measuring backscatter coefficients from time-gated echo signals appears in Ref. 1. The theory underlying that method is very general in terms of the applicability for broad ranges of experimental conditions. For example, the method can be applied for any combination of transducer-to-scattering-volume distance, duration and shape of the time gate, transducer geometry, and ultrasonic characteristics of the propagating medium.

Rigorous testing of the accuracy of the method was reported by Insana *et al.*[2] for the case of nonfocused disk-shaped transducers. These tests were performed using well-characterized scattering samples consisting of glass bead scatterers randomly distributed in an agar matrix. Backscatter coefficients for these samples were independently computed, based on the physical properties of the constituent materials, using the theory for individual particle scattering by Faran.[3] Experimentally determined backscatter coefficients were in excellent agreement with computed values (typically within about 10%) for a broad range of diagnostically useful frequencies. Backscatter coefficient measurements obtained using the method were also shown to be independent of transducer-to-scattering-volume distance for gate durations of 5 cycles or more.

Accurate gray-scale imaging of backscatter coefficients is an exciting application of the data reduction method, and use of focused transducers is important for resolution considerations. Use of focused transducers for making backscatter coefficient measurements on small samples *in vitro* is also important since appropriate volumes for measurement are often only a few cubic centimeters.

It is crucial, however, to verify experimentally the accuracy of the data reduction method for focused transducers, and this verification is the subject of the present paper. It has been recognized[4] that accurately accounting for pressure beams and other instrumental parameters is important in the data reduction. It is shown in this paper that our method of data reduction[1] maintains its accuracy for focused transducers over a broad range of transducer-to-scattering-volume distances for media with low attenuation and for media having attenuation mimicking that of tissues.

I. THE METHOD OF DATA REDUCTION

The method of data reduction is rigorously derived in Ref. 1. Following is a summary of the method for the convenience of the reader.

The experimental conditions used for measuring backscattered signals are illustrated in Fig. 1. An ultrasound transducer transmits an acoustic pulse into a sample and a portion of the received echo signal is gated and analyzed to obtain the backscatter coefficient. The data reduction method accounts for all physical aspects of the measurement process; thus the method includes an accurate model for the piezoelectric source and eliminates pulser–receiver characteristics through a thorough analysis of the echo from a reference reflector.

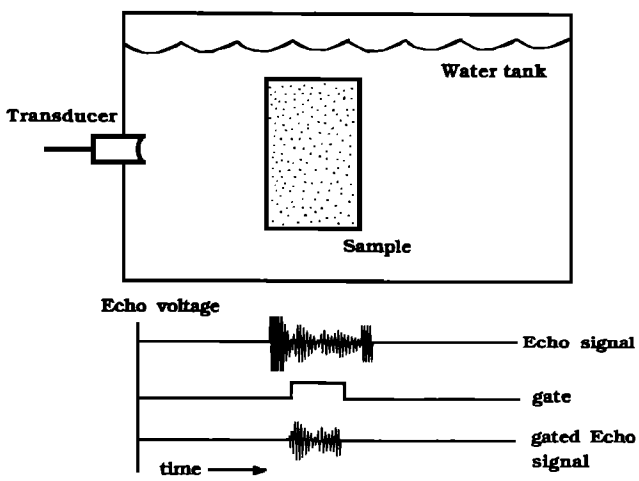

FIG. 1. Illustration of the experimental arrangement for recording echo signals. The scattering medium has planar surfaces perpendicular to the beam axis. Echo signal voltages are depicted along with a rectangular gate applied to the detected echo signal. The gated echo signal is sent to a transient recorder to be digitized and stored for later analysis.

[a] Present address: Department of Diagnostic Radiology, University of Kansas Medical Center, Kansas City, KS 66103.

[b] Present address: Department of Radiology, University of Missouri—Columbia Hospital and Clinics, Columbia, MO 65212.

 0001-4966/89/062410-07$00.80

The transducer is modeled as a set of equivalent point sources acting in unison and uniformly distributed over the active element of the transducer. Comparisons between this model and experiment show excellent agreement for pulsed and continuous wave fields beyond 3 or 4 cm from the transducer face.[5,6]

Two assumptions are made regarding the scattering medium. The first approximation is that the scattered wave fronts are assumed to be spherical in the region of the transducer face. Making this assumption implies that scattering is monopolar or that the scattering volume is sufficiently far from the transducer that angular variations in the scattered pressure waves over the receiving transducer are negligible. Second, it is assumed that the scatterers are randomly distributed in space but that the mean number of scatterers per unit volume is macroscopically uniform in the interrogated region.

The backscatter coefficient η at frequency ω_0 is given by

$$\eta(\omega_0) \simeq \left[\overline{\|V_s(\omega_0)\|^2} \Big/ \left(\frac{\tau}{2\pi}\right)^2 \iiint_{\Lambda} d\mathbf{r} \left| \int_{-\infty}^{\infty} d\omega \times T(\omega) B_0(\omega) \operatorname{sinc}\left(\frac{(\omega_0-\omega)\tau}{2\pi}\right) \times [A_0(\mathbf{r},\omega)]^2 \right|^2 \right], \quad (1)$$

where

$$A_0(\mathbf{r},\omega) \equiv \iint_S dS' \frac{e^{ik|\mathbf{r}-\mathbf{r}'|}}{|\mathbf{r}-\mathbf{r}'|}, \quad (2)$$

$V_s(\omega_0)$ is the Fourier transform of the gated echo signal evaluated at ω_0, and the bar denotes the mean value of several spatially uncorrelated measurements. The factors in the denominator account for the experimental conditions that affect the scattered signal. A rectangular time gate of duration τ is applied to the echo signal to select a scattering region of interest. The integral over volume Λ includes all scatterers in the pressure field; the region contributing to this integral is determined by the time gate and the pressure beam distribution. The integrand is the squared modulus of factors that include $T(\omega)$ as the receiver frequency response and $B_0(\omega)$ as a set of frequency-dependent superposition coefficients that give rise to the correct temporal acoustic pulse at any field point for the transducer employed. The sinc function corresponds to the rectangular time gate. [Recall that sinc $x \equiv (\sin \pi x)/\pi x$.] The vector $\mathbf{r} - \mathbf{r}'$ extends from the radiating element dS' to the field point. The surface of the radiating element is designated by S. For a single-element spherical cap transducer, the double integral can be reduced to a single integral.[5] (The term "spherical cap" here refers to a section of a spherical surface having a circular boundary.) The complex wavenumber in the propagating medium is defined as $k \equiv \omega/c(\omega) + i\alpha(\omega)$, where $c(\omega)$ is the ultrasonic speed and $\alpha(\omega)$ is the attenuation coefficient.

The echo from a planar reflector submerged in water and oriented with its reflecting surface perpendicular to the incident ultrasound beam is used to determine the product $T(\omega)B_0(\omega)$. Thus

$$T(\omega)B_0(\omega) = \frac{V_p(\omega)}{R \iint_S A_0(\mathbf{r},\omega) dS}, \quad (3)$$

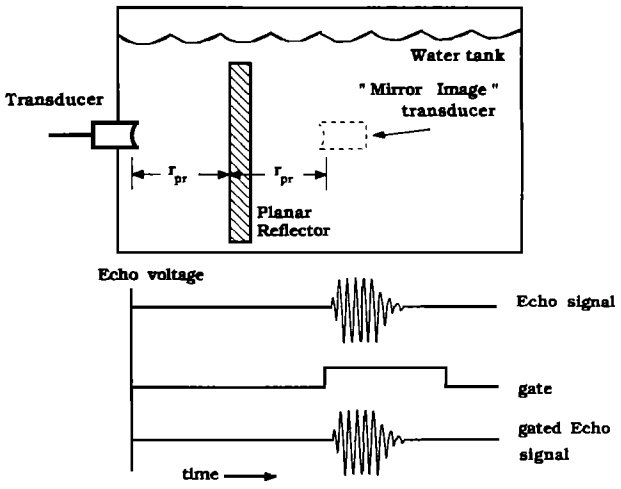

FIG. 2. Illustration of the experimental arrangement for collecting echo signals from a planar reference reflector for use in determining $T(\omega)B_0(\omega)$. A "mirror image" of the source transducer is shown at twice the source-to-reflector distance. The echo signal is depicted along with a rectangular gate applied to the echo signal showing the entire echo waveform is sent to the transient recorder.

where $V_p(\omega)$ is the Fourier transform of the echo voltage waveform and R is the amplitude reflection coefficient for the planar reflecting surface. The double integral in the denominator is over the surface of a "mirror image" transducer located at twice the transducer-to-planar reflector distance, as shown in Fig. 2.

II. TRANSDUCER PARAMETERS

To calculate the function $A_0(\mathbf{r},\omega)$ for a focused transducer, it is necessary to know the projected diameter and radius of curvature of its radiating element. As O'Neil has shown,[7] the directivity function[8] for a planar circular disk accurately describes the relative pressure amplitude in the "focal plane" of a weakly focused transducer driven by a sinusoidal voltage. The focal plane is defined as a plane perpendicular to the axis of symmetry of the radiating element and passing through the center of curvature of the radiating element. Agreement with the directivity function is unique to this plane, and this fact can be used to determine, experimentally, the radius of curvature and projected radius as described in Ref. 5.

The approximate radius of curvature of each transducer employed was given by the manufacturer. Scanning the pressure field in the appropriate region with a 1-mm hydrophone, we found the plane that yielded the best approximation to the directivity function of a disk transducer. The axial distance from the center of the transducer to this plane was taken to be the transducer's radius of curvature. The uncertainty in this distance is less than 1% based upon establishment of least minima between sidelobes. The first off-axis minima defining the mainlobe of the beam were then used to estimate the projected diameter. Propagating uncertainties in the positions of off-axis minima and radius of curvature yield an uncertainty in the effective transducer aperture of about 0.1 to 0.2 mm for the transducers used in this work. An example of the experimentally measured relative pressure is

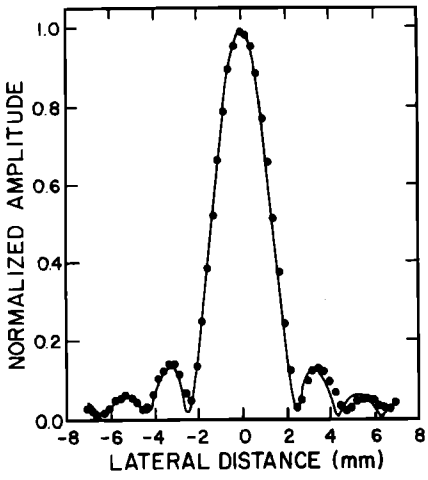

FIG. 3. Relative acoustic pressure amplitude values, shown as small circles, defining a lateral beam profile at an axial distance of 8.5 cm from a 5-MHz transducer excited by an approximately 40-wavelength, 5.0-MHz pulse. The solid line represents the directivity function chosen as a best fit to experimental measurements. The directivity function and measured values have been normalized to their respective peaks. These data allow determination of the radius of curvature and projected diameter of the transducer.

shown in Fig. 3 along with a directivity function fitting the experimental data. The directivity function and the measured relative pressure have been normalized to their respective peaks. The nominal transducer frequency as well as the carrier frequency of the pulse was 5.0 MHz. The measured profile follows the directivity function quite well. The absence of completely zero values between sidelobes is likely the result of electronic noise or the fact that the hydrophone perturbs the pressure field.

This procedure was used to determine the radius of curvature and effective aperture for three transducers employed in this work. Table I shows the nominal resonant frequency, radius of curvature, and effective transducer aperture for each transducer. In each case, the carrier frequency of the narrow-band pulses used to determine the projected diameter and radius of curvature was chosen to equal the nominal frequency specified by the manufacturer.

III. SCATTERING MATERIALS

Two phantoms were used in this study, one a cylinder (13-cm diameter, 6 cm thick), called phantom 1, and the other a rectangular parallelepiped ($6\times13\times16$ cm), called phantom 2. Both have parallel 50-μm-thick Saran Wrap™ acoustic windows. The scattering medium in both phantoms consists of glass bead scatterers randomly positioned in an agar matrix such that the mean number per unit volume is uniform. The scatterers in phantom 1 have a narrow diameter distribution with a mean diameter of 57.4 μm. Measurements for estimating the diameter distribution were done using an optical microscope with a calibrated ocular micrometer. A histogram of the diameter distribution is shown in Fig. 4 for a cluster of 139 particles in this slab. Mean concentrations of scatterers were found by counting the number of beads in a thin slab of the sample and dividing by the volume of the slab. The latter volume was obtained indirectly by accurately measuring its mass and density. The resulting mean scatterer concentration is $\overline{N} = 7.7 \pm 0.2$ scatterers/mm.[3] The uncertainty in $\overline{N}$ is based primarily on the limited number of beads counted; this number was 996, and assuming Poisson statistics, the uncertainty is $\pm$ 3%. Note that it is reasonable to assume the existence of a microscopically random distribution of scatterers and uniformity of the mean number of scatterers per unit volume in the phantoms ("macroscopic uniformity"). This assumption is based on two facts. First, since the measured mean number of scatterers per unit volume is 7.7 mm^{-3}, the mean distance between nearest scatterers is roughly 500 μm, which is large compared to the mean scatterer diameter of 57.4 μm. Second, in the manufacturing technique, the scatterers are stirred evenly into the viscous molten agar, and the ensuing congealing occurs during constant rotation of the material about a horizontal axis at 2 revolutions/min. Also, *B* scans of the completed phantoms through different scanning windows corroborate the assumption of macroscopic uniformity.

Phantom 2 is very similar to phantom 1. The mean diameter of the glass bead scatterers is about the same as that in phantom 1. In addition, very finely powdered graphite is uniformly distributed throughout the phantom, raising the frequency-dependent attenuation to one typical of most soft tissues.[9] The graphite particles are small enough that their

TABLE I. Values of radii of curvature and projected diameter for the three transducers employed in this work. These parameters were determined from lateral beam profile measurements as in Fig. 3. In each case, the carrier frequency of the narrow-band pulses employed was chosen to equal the nominal frequency.

Transducer parameters		
Nominal resonant frequency (MHz)	Radius of curvature (cm)	Effective aperture (mm)
2.25	13.7 $\pm$ 0.7	18.3 $\pm$ 0.1
3.5	9.65 $\pm$ 0.07	19.2 $\pm$ 0.2
5.0	8.50 $\pm$ 0.06	18.6 $\pm$ 0.02

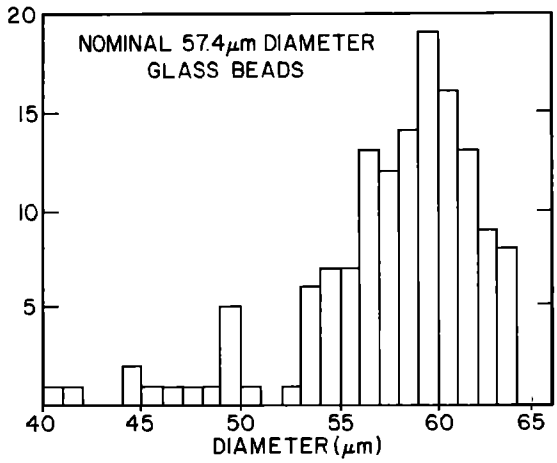

FIG. 4. Histogram of the glass bead diameter distribution in the low-attenuating phantom. The diameters were measured using an optical microscope equipped with a calibrated ocular micrometer. The total number of beads counted in forming this histogram was 139.

contribution to the backscatter coefficient is negligible compared to that of the glass beads. This fact was verified using a sample containing graphite powder, but no glass beads.

Ultrasonic speeds and frequency-dependent attenuation coefficients were measured using a through transmission technique[9] at 20 °C. Ultrasonic speeds were measured at a single frequency, and the attenuation was measured at five discrete frequencies between 1 and 7 MHz. Attenuation coefficients were then curve fitted assuming the functional form

$$\alpha(\omega) = \alpha_1\omega + \alpha_2\omega^2,$$

where ω is frequency and α_1 and α_2 are constants. The small dependence of ultrasonic speed on frequency was determined using the Kramers–Kronig relation given by Ginzberg[10] and was used in computing the complex wavenumber. Ultrasonic speeds, attenuation coefficients, and densities for both phantoms are given in Table II.

Backscatter coefficients for these phantoms were computed independently using the theory of Faran. Required parameters for the glass beads were the density (2.4 g/cm^3), Poisson's ratio (0.21) and the longitudinal speed of sound (5570 m/s) (see Ref. 11). The density and ultrasonic speed of the media surrounding the beads are given in Table II. Backscatter coefficients were computed for each particle size in the distribution (such as shown in Fig. 4), and these results were combined in a weighted sum as described in Ref. 2.

IV. EXPERIMENTAL APPARATUS AND PROCEDURE

Figure 5 shows a block diagram of the experimental apparatus for measuring backscatter coefficients. This apparatus is very similar to that described in Ref. 2 with refinements involving the transient recorder, computer, and a computer-controlled three-axis positioning device. A signal generator was used to create 5-μs sinusoidal pulses. These pulses were then amplified and used to drive the transducer. The pulse repetition frequency was adjusted so that all echoes from the phantom due to one pulse were received before the next pulse occurred. A stepless electronic gate, 10 μs in duration, was used to select echo signals corresponding to a region of interest. A broadband receiver amplifier was used to raise the echo signals to several hundred millivolts peak to peak. The gated signals were then digitized and stored for off-line analysis.

TABLE II. Density and ultrasonic properties of the two phantoms used in this work. The attenuation coefficient is described in terms of two constants, α_1 and α_2, corresponding to a curve fitting to experimental values of the form $\alpha(\omega) = \alpha_1\omega + \alpha_2\omega^2$.

Phantom	Attenuation coefficient α_1 dB/cm MHz	Attenuation coefficient α_2 dB/cm MHz^2	Speed of sound m/s	Density g/cm^3
1 Low attenuating	0.046	0.013	1532 ± 3 (2.00 MHz)	1.00 ± 0.005
2 Tissuelike attenuating	0.48	0.018	1525 ± 3 (2.50 MHz)	1.04 ± 0.005

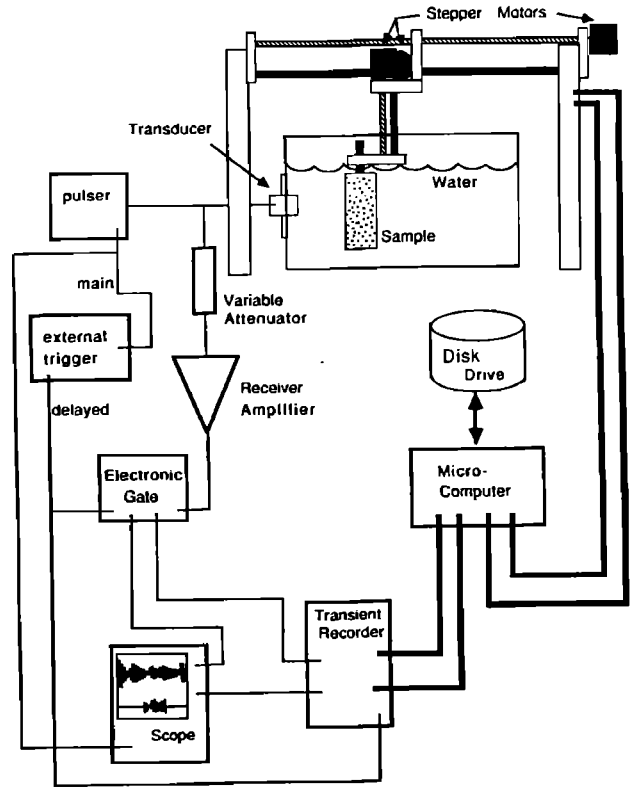

FIG. 5. Block diagram illustrating the experimental apparatus used to determine acoustic backscatter coefficients. A waveform generator is used to excite the transducer with 5-μs pulses. Received echo signals are amplified, gated, and digitized. The digitized echo signals are stored on a computer for off-line analysis. Synchronization of all devices is maintained with an external trigger. Stepper motors are used to translate the scattering sample between recordings.

Backscatter coefficient determination involves recording two separate types of echo signals. First, a planar reference reflector is employed to determine the product $T(\omega)B_0(\omega)$, as shown in Eq. (3). The reference reflector used was a Lucite™ block approximately 15×20 cm in reflecting area and thick enough that the echo waveform from the proximal surface did not overlap that from the distal surface. Care was taken to align the interface perpendicular to the beam axis employing a micrometer-driven, dual-axis orienting device to maximize the echo signal amplifier. In repeated measurements of planar reflector signals, we have found that accurate determination of $T(\omega)B_0(\omega)$ can be made with the planar reflector at any axial position, but the precision of this determination appears to be highest when the reflecting surface is located at the transducer's radius of curvature.

Initially, backscatter coefficient measurements were made with the phantom at different axial distances from the transducer, the interrogated volume being a couple of centimeters from the proximal scanning window. For each transducer-to-scattering-volume distance, gated echo signals were recorded at 50 to 70 statistically independent positions by lateral translations of the phantom between recordings.

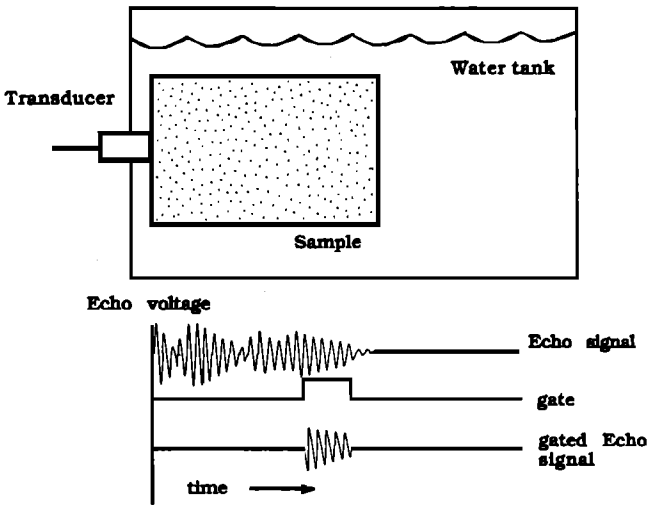

FIG. 6. Illustration of the experimental arrangement in which the phantom is maintained in direct contact with the transducer. Echo signal voltages are depicted along with a rectangular gate applied to the detected signal. Gated echo signals are sent to a transient recorder to be digitized and stored for later analysis.

Discrete Fourier transforms of each of these 50–70 waveforms were then computed yielding the values of $V_s(\omega_0)$. The mean value of the squared moduli of these Fourier transforms then yields the numerator of Eq. (1), viz., $\overline{\|V_s(\omega_0)\|^2}$.

Further tests involved a second experimental arrangement, shown in Fig. 6, in which phantom 2 was in contact with the transducer face and tissuelike attenuation was present over the full acoustic path. This setup mimics typical *in vivo* studies and is another important step toward clinical application of backscatter coefficient measurements.

To test the accuracy of the method over a broad range of frequencies, backscatter coefficients were determined at ten frequencies in the range from 2–6 MHz using phantom 1. All three focused transducers were employed. In each case, the

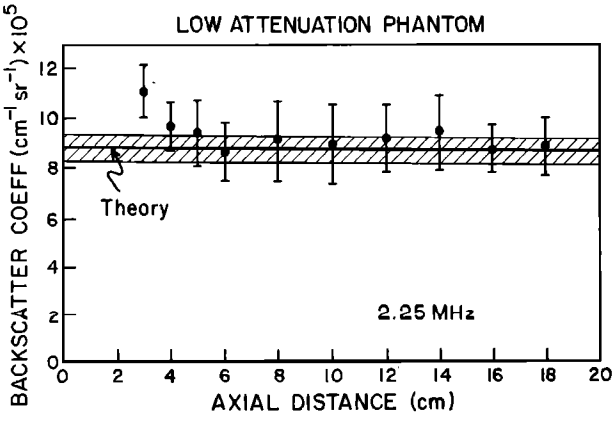

FIG. 7. Experimental values of the backscatter coefficient $\eta(\omega_0)$ for phantom 1 (low attenuation) at various transducer-to-scattering-volume distances using the nominal 2.25-MHz transducer at $\omega_0 = 2.25$ MHz. The error bars correspond to our estimate of the uncertainty. The pulse and gate durations were 5 and 10 μs, respectively. The horizontal cross-hatched band corresponds to the predicted value based on Faran's theory[3] $\pm$ our estimate of the uncertainty (accuracy).

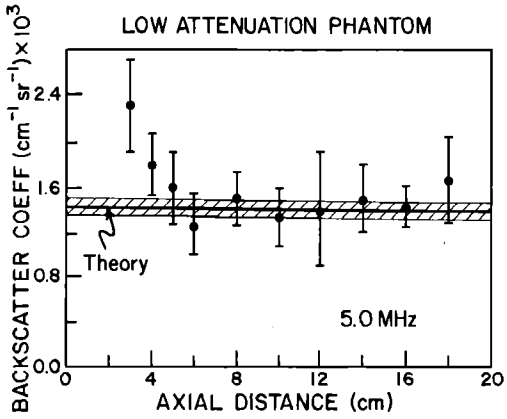

FIG. 8. Experimental values of $\eta(\omega_0)$ for phantom 1 (low attenuation) at various transducer-to-scattering-volume distances using the nominal 5-MHz transducer at $\omega_0 = 5.0$ MHz. All other parameters are the same as described for Fig. 7.

volume interrogated was in the focal region of the transducer. The 2.25-MHz transducer was used at frequencies of 2.0, 2.25, 2.5, and 3.0 MHz; the 3.5-MHz transducer was used at frequencies of 3.5 and 4.0 MHz; and the 5-MHz transducer was used at frequencies of 4.5, 5.0, 5.5, and 6.0 MHz.

Additional details regarding experimental and numerical methods can be found in Refs. 1 and 2.

V. RESULTS

Backscatter coefficients η obtained for various experimental situations are shown in Figs. 7–11. In Figs. 7–10, the frequency at which η was determined was either 2.25 or 5.0 MHz employing the transducers with nominal frequencies of 2.25 and 5.0 MHz, respectively. In each figure, error bars correspond to our estimate of the total uncertainty (accuracy, as opposed to precision) in the measured value. This total uncertainty includes the standard deviation of the mean[12] of $\|V_s(\omega_0)\|^2$ combined, using the standard method for propa-

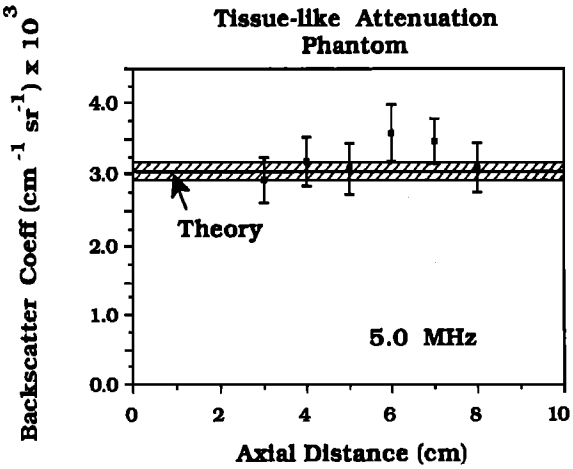

FIG. 9. Experimental values of $\eta(\omega_0)$ for phantom 2 (tissuelike attenuation) at various transducer-to-scattering-volume distances using the nominal 5-MHz transducer. All other parameters are the same as given for Fig. 8.

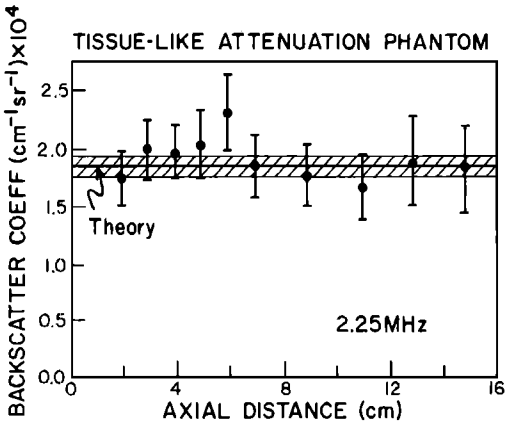

FIG. 10. Experimental values of $\eta(\omega_0)$ for phantom 2 in contact with the transducer as shown in Fig. 6. An electronic gate was used to pass signals only from a desired depth of interest. All other parameters are the same as for Fig. 7.

gation of errors,[12] with instrumental uncertainties in measurements of medium attenuation coefficients and transducer diameters and radii of curvature. The uncertainty in $\overline{\|V_s(\omega_0)\|^2}$ dominates in most cases, that due to the attenuation coefficient becoming comparable only for the most distal values of η (on the right) in Fig. 10. The horizontal cross-hatched bar in each figure corresponds to the backscatter coefficient computed using the theory of Faran as described in Refs. 1 and 2. (The computed value is at the center of the bar and the height of the bar corresponds to the estimated uncertainty in that value; a discussion of the basis for this accuracy estimate is given in Sec. VI.)

Figures 7 and 8 show backscatter coefficients measured at 2.25 and 5.0 MHz, respectively, for phantom 1. Here, η is plotted for a broad range of transducer-to-scattering-volume distances, viz., 3–18 cm. In both cases, the volume interrogated was a few centimeters beyond the proximal scanning window, as depicted in Fig. 1.

Figure 9 shows a plot of η versus transducer-to-scattering-volume distance using phantom 2, the interrogated volume again always being a few centimeters from the proximal scanning window. Measurements were made at 5.0 MHz and for depths ranging from the nearfield into the focal region.

Figure 10 shows a plot of results at 2.25 MHz with phantom 2 and the transducer being maintained in contact with the phantom for all depths interrogated, as depicted in Fig. 6. Thus η was measured at depths from 2 to 15 cm with tissuelike attenuation present over the entire acoustic path.

In Fig. 11 are shown values of η for phantom 1 measured over a range of frequencies from 2–6 MHz.

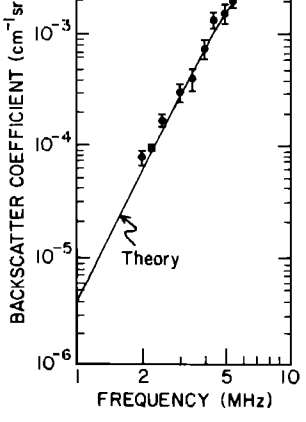

FIG. 11. Theoretical and experimental values for the backscatter coefficient at ten frequencies from 2–6 MHz for phantom 1. Three transducers with nominal frequencies of 2.25, 3.5, and 5.0 MHz were used. The theoretical values (solid line) were predicted using Faran's theory.[3] The uncertainty (accuracy) in the Faran values is ± 0.06 at any frequency.

VI. DISCUSSION

The accuracy of the backscatter coefficients determined experimentally was discussed in the previous section. It is also important to discuss our estimate for the accuracy of the values computed using the theory of Faran. The value was computed using the expression

$$\eta_{\text{theory}}(\omega_0) \cong \sum_{i=1}^{L} f_i \eta_i(\omega_0) , \tag{4}$$

where ω_0 is the frequency of concern, i corresponds to the ith diameter bin of the histogram in Fig. 4, f_i corresponds to the number fraction in the ith bin (e.g., $f_i = 19/139$ in the bin between 59 and 60 μm), and $n_i(\omega_0)$ is a backscatter coefficient computed assuming all scatterers have the diameter centered in the ith bin. The upper limit L on the sum equals the number of diameter bins.

The accuracy of the value obtained using Eq. (4) improves as the number of beads having their diameters measured increases. The right side of Eq. (4) equals the mean value of the η_i's; therefore, the uncertainty in η_{theory} due to the small sample number (139 in Fig. 4) equals the standard deviation of the mean,[12] viz.,

$$\sigma_{\text{mean}} = \sqrt{\left[\left(\sum_{i=1}^{L} N_i(\eta_i - \bar{\eta})^2\right) \Big/ N(N-1)\right]} , \tag{5}$$

where

$$\bar{\eta} \equiv \sum_{i=1}^{L} f_i \eta_i(\omega_0) \equiv \left(\sum_{i=1}^{L} N_i \eta_i(\omega_0)\right) \Big/ N \tag{6}$$

is the sample mean, N_i is the number of beads in the sample in the ith bin, and $N \equiv \Sigma_{i=1}^{L} N_i = 139$. Inserting values of η_i computed using the Faran theory and $\bar{N} = 7.7\ \text{mm}^{-3}$, the fractional error in $\bar{\eta}$—and, therefore, in η_{theory}—due to the limited sample number is $\sigma_s/\bar{\eta} = 0.03$. Nearly the same fractional error resulted from the corresponding analysis involving the diameter distribution corresponding to phantom 2.

The uncertainty in the Faran value also depends on the uncertainty in the mean number of particles per unit volume $\bar{N}$, ($\pm 3\%$), and on the uncertainties in values of physical parameters for the beads and the supporting agar-based medium. For the glass composing the beads, these uncertainties include those in the longitudinal ultrasonic speed ($\pm 2\%$), the density ($\pm 1\%$), and the Poisson's ratio ($\pm 25\%$). For the supporting agar-based medium, uncertainties in the density ($\pm 0.5\%$) and in the ultrasonic speed ($\pm 0.2\%$) were also accounted for. The above uncertainties are propagated through the η_i values of Eq. (4). The net fractional uncertainty in η_{theory} due to the above uncertainties in $\bar{N}$ and material physical properties is ± 0.05.

Finally, the total fractional uncertainty in η_{theory} due to all factors is $\pm\sqrt{(0.03)^2 + (0.05)^2} = \pm 0.06$. This fractional uncertainty defines the height of the cross-hatched horizontal band in Figs. 7–10.

For almost all experimental situations, very good agreement was found between experimentally determined backscatter coefficients and those predicted using the theory of Faran (which employs bulk physical properties of spheres and their surroundings). However, in the case of the low-attenuation phantom (see Figs. 7 and 8), there was a tendency for the experimental values to become elevated as the transducer-to-scattering-volume distance was decreased below 4 or 5 cm. The elevation above the theoretical values is significant only at 3 cm for both the 2.25-MHz case (Fig. 7) and the 5-MHz case (Fig. 8), and this elevation is more pronounced at 5 MHz. As shown in Figs. 9 and 10, this phenomenon was not manifested in the case of phantom 2 in which the attenuation mimics soft tissue. However, there does appear to be a slight elevation in the experimentally determined backscatter coefficient at an axial distance of about 6 cm in Figs. 9 and 10. It is possible that this elevation is related to that in the case of Figs. 7 and 8. However, at this writing, we have no explanation for any of the elevations discussed.

The ability to accurately measure backscatter coefficients employing focused instead of nonfocused transducers allows significant reduction in the volume of material necessary to estimate this parameter or, conversely, to increase the amount of data available from a given volume. When this is combined with the broad range of transducer-to-scattering-volume distances available, formation of accurate grey-scale backscatter coefficient images is facilitated in which the resolution is reasonably good. Formation of such images is the subject of another paper.[13]

VII. CONCLUSIONS

Using phantoms with low or tissuelike attenuation, we have verified that the method of data reduction employed in this work accurately determines backscatter coefficients for the following combination of experimental conditions: (1) use of focused transducers; (2) transducer-to-scattering-volume distances extending from the near field through the farfield of the pressure beam; (3) relatively narrow-band pulses and long gate durations; and (4) frequencies in the diagnostic ultrasound range.

ACKNOWLEDGMENTS

This work was supported in part by NIH Grants R01-CA39224 and R01-CA25634.

[1]E. L. Madsen, M. I. Insana, and J. A. Zagzebski, "Method of data reduction for accurate determination of acoustic backscatter coefficients," J. Acoust. Soc. Am. **76**, 913–923 (1984).

[2]M. F. Insana, E. L. Madsen, T. J. Hall, and J. A. Zagzebski, "Tests of the accuracy of a method of data reduction for determination of acoustic backscatter coefficients," J. Acoust. Soc. Am. **79**, 1230–1236 (1986).

[3]J. J. Faran, Jr., "Sound scattering by solid cylinders and spheres," J. Acoust. Soc. Am. **23**, 405–418 (1951).

[4]Y. W. Yuan and K. K. Shung, "The effect of focusing on ultrasonic backscatter measurements," Ultrason. Imag. **8**, 121–130 (1986).

[5]E. L. Madsen, M. M. Goodsitt, and J. A. Zagzebski, "Continuous waves generated by focused radiators," J. Acoust. Soc. Am. **70**, 1508–1517 (1981).

[6]M. M. Goodsitt, E. L. Madsen, and J. A. Zagzebski, "Field patterns of pulsed focused radiators in attenuating and nonattenuating media," J. Acoust. Soc. Am. **71**, 318–329 (1982).

[7]H. T. O'Neil, "Theory of focusing radiators," J. Acoust. Soc. Am. **21**, 516–526 (1949).

[8]L. E. Kinsler, A. R. Frey, A. B. Coppens, and J. V. Sanders, *Fundamentals of Acoustics* (Wiley, New York, 1982), p. 453.

[9]E. L. Madsen, J. A. Zagzebski, R. Banjavic, and R. Jutila, "Tissue mimicking materials for ultrasound phantoms," Med. Phys. **5**, 391–394 (1978).

[10]V. L. Ginzberg, "Concerning the general relationship between absorption and dispersion of sound waves," Soviet Phys. Acoust. **1**, 32–41 (1955).

[11]Glass bead density was measured in our lab using water displacement in a graduated cylinder with a large mass of glass beads. Poisson's ratio and the longitudinal speed of sound were calculated from parameters supplied by the manufacturer (Potter's Industries).

[12]P. R. Bevington, *Data Reduction and Error Analysis for the Physical Sciences* (McGraw-Hill, New York, 1969), pp. 72 and 116.

[13]E. J. Boote, J. A. Zagzebski, E. L. Madsen, and T. J. Hall, "Instrument independent acoustic backscatter imaging," Ultrason. Imag. **10**, 121–138 (1988).